Guo *et al. Journal of Translational Medicine* (2025) 23:542
https://doi.org/10.1186/s12967-025-06423-4

Journal of
Translational Medicine

RESEARCH

Open Access

Mitochondrial dysfunction fuels drug resistance in adult T-cell acute lymphoblastic leukemia

Shanshan Guo[1,2,3], Ekaterina Bourova-Flin[2,3], Sophie Rousseaux[2,3], Florent Chuffart[2,3], Lijun Peng[1,3], Duohui Jing[1], Jian-Qing Mi[1,3], Saadi Khochbin[2,3*] and Jin Wang[1,3*]

Abstract

Background T-cell acute lymphoblastic leukemia (T-ALL) is a relatively rare hematological malignancy, characterized by the uncontrolled proliferation of immature T lymphoblasts and associated with a generally unfavorable prognosis. Our previous research has demonstrated that decreased mitochondrial activity is associated with the aggressiveness of T-ALL tumors. However, the mechanisms underlying this phenomenon and its contribution to treatment resistance remain largely elusive.

Methods We have built up the largest known T-ALL tumor bank, with a median follow-up of 32 months, including our transcriptomic data from 79 newly sequenced tumors that adds to the 54 publicly accessible samples. Computational analyses and a series of functional assays were performed to investigate the molecular links between altered mitochondrial activity and drug resistance.

Results The transcriptomic analysis revealed that down-regulation of mitochondrial activity is a potent driver of *ABCB1* activation, a gene strongly associated with multidrug resistance. In tumors with low mitochondrial activity, the impaired fatty acids β-oxidation leads to intracellular lipid accumulation, which is directly involved in *ABCB1* activation. Indeed, our data show that lipid neo-synthesis and accumulation promotes the activation of lipogenic transcription factors, liver X receptors (LXRs), which act as drivers of *ABCB1* expression. Tumor data analyses confirmed that high *ABCB1* expression in tumour samples is indeed associated with reduced mitochondrial gene expression, lipid droplet enrichment, increased tumour aggressiveness, and significantly shorter patient survival.

Conclusions Our study demonstrates that reduced mitochondrial activity drives multidrug resistance in adult T-ALL via lipid-mediated activation of *ABCB1*. These findings enhance our understanding of the biology of aggressive T-ALL and provide insight into mechanisms of resistance to conventional chemotherapy. Consequently, we propose that targeting de novo lipogenesis and restricting dietary fats, such as caprylic acid, may help overcome treatment resistance in patients with T-ALL exhibiting low mitochondrial activity.

Trial registration The clinical trial was registered under the identifiers ChiCTR-ONRC-14004968 and ChiCTR2000031553 at ClinicalTrials.gov.

*Correspondence:
Saadi Khochbin
saadi.khochbin@univ-grenoble-alpes.fr
Jin Wang
jinwang@shsmu.edu.cn; saadi.khochbin@univ-grenoble-alpes.fr
Full list of author information is available at the end of the article

Keywords T-cell acute lymphoblastic leukemia, Mitochondrial activity, *ABCB1* activation, Lipid accumulation, Drug resistance

Background

T-cell acute lymphoblastic leukemia (T-ALL) represents a relatively rare and heterogeneous group of hematologic malignancies that account for 20–25% of ALL in adults, with an incidence rate of less than 10 individuals per million [1–4]. This type of disease originates from T cell precursors halted at specific stages of differentiation [1]. The proliferation and accumulation of leukemic blasts in the bone marrow can suppress normal hematopoiesis, resulting in anemia, thrombocytopenia and neutropenia, along with corresponding clinical symptoms [5]. Additionally, primitive T-lymphocytes may also accumulate in various extramedullary sites, especially in the cerebrospinal fluid, gonad, thymus, liver, spleen and lymph nodes. Research on adult T-ALL has been comparatively less extensive than that on its more common pediatric counterparts [6]. In recent years, although complete remission (CR) can be achieved in most patients with ALL (especially in children), adult patients with T-ALL frequently encounter difficulties such as resistance to primary chemotherapy and early relapse, resulting in a dismal prognosis [3]. Despite the high rate of induction failure in adult T-ALL, little is known about the factors that predict resistance and affect outcomes. This is primarily due to the small cohort sizes in clinical studies, variations in patient ethnicity, differences in treatment protocols across trials, and a limited understanding of pathogenesis, among other factors.

The establishment of statistically significant cohorts of adult T-ALL was urgently needed to enhance our understanding of the molecular basis of this deadly pathology. Therefore, we concentrated our efforts on adult T-ALL because of its unique biological characteristics, treatment responses, and clinical outcomes compared to pediatric cases. These differences necessitate a specialized approach to effectively understand and manage the disease in adult patients.

Previously, by considering aberrant tissue-specific gene activation, using published adult and pediatric T-ALL transcriptomic data [7], we defined a 5 gene expression classifier (GEC) capable of identifying aggressive, treatment resistant adult and children T-ALL tumours [8]. By studying the biological characteristics of these aggressive tumours on the basis of this GEC signature, we were able to demonstrate that the tumours of patients with a shorter survival time (GEC positive) are depleted in genes encoding mitochondrial proteins. We also found that this biological characteristic was also true for patients presenting "minimal residual disease" (MRD positive), most of which are GEC positive [8]. These data, indicated that the impairment of mitochondrial activity in these cancers is one of the characteristics of aggressive tumours. However, these studies did not allow to determine the molecular basis of tumour aggressivity associated with mitochondria depletion. To this aim, we first significantly increased our adult T-ALL tumour whole RNA sequencing to include additional 79 tumours from patients with well-annotated clinical data to reach a total of 133 samples including the previously reported transcriptome of 54 samples [7].

Using this large series of adult T-ALL samples transcriptomic data, we investigated the biological impact of mitochondrial activity impairment and the molecular basis of tumour resistance to induction chemotherapy. Our data pointed to lipid-mediated activation of *ABCB1* gene, encoding the multidrug resistant protein P-gp (MDR1). Low mitochondrial activity systematically induced *ABCB1* due to lipid accumulation and the activation of LXR transcription factors. Additionally, we also found that in mitochondria depleted cells, dietary lipids also efficiently induced *ABCB1* gene expression. These data not only uncover the prominent biological features of aggressive T-ALL tumours, but also suggest that inhibition of de novo lipogenesis and avoiding dietary lipids for patients with lower mitochondrial activity could impact tumour resistance to induction chemotherapy.

Materials and methods

T-ALL patients and samples collection

Bone marrow (BM) samples containing high percentages of leukemic blasts from newly-diagnosed adult T-ALL patients were collected at the Hematology Department of Ruijin hospital, Shanghai Jiaotong university school of medicine. Diagnoses were assigned based on the World Health Organization Classification of Haematolymphoid Tumours: Lymphoid Neoplasm and NCCN Guidelines Version 2.2024-Acute Lymphoblastic Leukemia [9]. This study recruited 133 adult T-ALL patients (median age, 33 years) between February 2009 and January 2022 treated on the ChiCTR-ONRC-14004968 and ChiCTR2000031553 trials. A signed written informed consent for research use was obtained for each patient in accordance with the Declaration of Helsinki, approved by the Ethics Review Committee of Ruijin Hospital.

Immunophenotype was ascertained by multiparameter flow cytometric characterization from BM aspirates at initial diagnosis using a FACScan instrument (Becton–Dickinson, San Jose, California). Available characteristic information including age at diagnosis, gender, cytogenetic abnormalities and flow cytometry-based characterizations of these primary T-ALL samples are listed in Table 1. BM samples from T-ALL patients were obtained in heparin-coated vacutainers. Leukemia mononuclear cells from BM samples were isolated after Ficoll (Axis-Shield, AS1114546) gradient centrifugation, then stored at −80 °C or were frozen in fetal bovine serum with 10% dimethylsulfoxide (DMSO) and preserved in liquid nitrogen for further use.

All patients were treated with conventional intensive induction, consolidation and maintenance chemotherapy. For the assessment of clinical events and outcomes, CR was characterized by bone marrow blasts < 5% and complete hematologic recovery [absolute neutrophil count (ANC) $\geq 1\times10^9$/L, platelet count $\geq 100\times10^9$/L], and no accompanying extramedullary disease. MRD was evaluated by multicolor flow cytometry, with MRD considered negative if fewer than 0.01% lymphoblasts were detected (cutoff 10^{-4}) in BM samples. Relapse was defined as reappearance of blasts in the blood or bone marrow exceeding 5%, or in any extramedullary site after achieving CR. Progression was defined as relapse or a minimum 25% increase in the absolute number of circulating or BM blasts or emergence of extramedullary disease or death. Prespecified primary endpoints were objective remission rate and survival probabilities.

Table 1 Baseline characteristics of adult T-ALL patients (n = 133)

Characteristics	Total (N = 133)
Sex	
Female	42 (31.58%)
Male	91 (68.42%)
Age (yr)	33 (22.5–47.5)
Ethnicity	
Chinese	133 (100%)
Blasts% at diagnosis	88.1 (76–92.5)
WBC, × 10^9/L	25.77 (6.2–94.245)
≤ 100	101 (75.94%)
> 100	32 (24.06%)
HB, g/dL	106 (80–133)
PLT, × 10^9/L	91 (42–168)
Immunologic classification	
Pro	50 (37.59%)
Pre	42 (31.58%)
Cortical	32 (24.06%)
Medullary	9 (6.77%)
ETP/non-ETP status	
ETP	54 (40.60%)
Near-ETP	8 (6.02%)
Non-ETP	71 (53.38%)
Molecular subtypes	
NOTCH1	86 (64.66%)
FBXW7	31 (23.31%)
RAS	31 (23.31%)
PTEN	7 (5.26%)
Cytogenetics	
0–2 abn	86 (64.66%)
CK ≥ 3	22 (16.54%)
NA	25 (18.80%)
CNS involvement	15 (11.28%)
Response to therapy	
CR at any time point	101/119 (84.87%)
Relapse	29/101 (28.71%)
Progression	73 (54.89%)
Bridge to HSCT	62 (46.62%)

Results were expressed as number of cases (percentage, %) or median (IQR (P25, P75))

WBC white blood cell count; *HB* hemoglobin; *PLT* platelet; *ETP* early T cell precursor; *abn* abnormalities; *CK* complex karyotype; *CNS* central nervous system; *CR* complete remission; *HSCT* hematopoietic stem cell transplantation; *IQR* interquartile range; *NA* Not available

Cell culture and materials

The human acute T lymphoblastic leukemia cell lines CCRF-CEM (ATCC#CCL-119), MOLT-4 (ATCC#CRL-1582), JURKAT (ATCC#TIB-152), LOUCY (ATCC#CRL-2629) and SUP-T1 (ATCC#CRL-1942) used in our study were originally purchased from ATCC website. 6T-CEM cell line was obtained from Shanghai Institute of Hematology (Shanghai, China). Each cell line identity was verified by STR profiling (GENETIC TESTING BIOTECHNOLOGY) before experiments. All of these cell lines were maintained in RPMI-1640 medium with GlutaMAXTM-I (Gibco, 6170-044) supplemented with 10% fetal bovine serum (Gibco, 10270-106) and 1× streptomycin/penicillin antibiotics (Gibco, 151140-122) at 37 °C in a humidified 5% CO_2 atmosphere. Routine testing ensured the absence of mycoplasma contamination in the cells.

CCRF-CEM cells and MOLT-4 cells were continuously exposed to 200ng/mL, 100ng/mL ethidium bromide (EtBr), respectively, for 7 days to deplete mtDNA. Culture medium was supplemented with uridine (50μg/mL, Sigma, U3003) and sodium pyruvate (1mM, Sigma, S8636) to maintain living cells with dysfunctional mitochondria.

The following chemical reagents were used for in vitro experiments: Ethidium bromide (Sigma, E1510), Chloramphenicol (Sigma, C0378), Vincristine sulfate (Selleck, S1241), Cytarabine (Selleck, S1648), Octanoate (Sigma,

C5038), Ranolazine (Sigma, R6152), ND-630 (MedChemExpress, HY-16901), GSK2033 (MedChemExpress, HY-108688), GW3965 (MedChemExpress, HY-10627A), Tariquidar (Selleck, S8028). Drug concentration and treatment time are indicated in respective figure legends.

mtDNA-qPCR detection of mtDNA levels

Relative mtDNA copy number was determined using a quantitative real-time PCR method (mtDNA-qPCR). This assay quantifies relative mtDNA levels by assessing the ratio of mitochondrial copy number to single-copy nuclear gene. Genomic DNA from T-ALL cell lines was extracted by utilizing DNeasy Blood & Tissue Kit (QIAGEN, 6904) or AllPrep DNA/RNA/Protein Mini Kit (QIAGEN, 80004). A total of 5ng DNA was added as template for each reaction in a total volume of 10μl, qPCR was completed using SYBR Green (TaKaRa, RR420A) on the q-PCR ViiA 7 platform (Thermo Fisher, USA). Primer sequences (Sangon Biotech; Eurogentec) used in this study are as follows: mt-CO1, 5′-ATACTACTA ACAGACCGCAACCTC-3′ and 5′-GAGATTATTCCG AAGCCTGGT-3′; n-BACTG, 5′-GAAGGATTCCTA TGTGGGCGA-3′ and 5′-CAGGGTGAGGATGCCTCT CTT-3′ [10]; mt-tRNA^{Leu}, 5′-CACCCAAGAACAGGG TTTGT-3′ and 5′-TGGCCATGGGTATGTTGTTA-3′; n-B2M, 5′-TGCTGTCTCCATGTTTGATGTATCT-3′ and 5′-TCTCTGCTCCCCACCTCTAAGT-3′ [11]. The 2 pairs of mtDNA primers (mt-CO1, mt-tRNA^{Leu}) for qPCR assays were specifically designed to amplify unique regions of the mitochondrial genome, avoiding sequences with high homology to NUMTs (nuclear mitochondrial DNA sequences) through BLAST analysis against the nuclear genome [12]. Primer specificity was further verified using mitochondrial DNA from purified mitochondria. Negative controls without template DNA were included to exclude non-specific amplification. Amplification efficiency and specificity were confirmed by melt curve analysis with single peaks, ensuring the signals primarily reflect mtDNA content. Finally, mtDNA genomic copies were calculated using $2^{-\triangle Ct}$ method.

Apoptosis assay

To distinguish apoptotic or necrotic cells, we harvested 1×10^6 T-ALL cells per condition 48 h after treatment with vehicle (DMSO), VCR, Ara-C. FITC-Annexin V and propidium iodide (BD, 556547) were added to stain cells for 10 min at room temperature prior to acquisition on the flow cytometer (the LSR Fortessa TM X-20 flow cytometer, BD). FlowJo v10 was used for analyzing data. Proportion of drug-induced apoptosis was estimated by comparing T-ALL cells treated with DMSO alone.

Western blot analysis

Approximately 5×10^6 cells were collected and washed twice with cold 1×PBS, total cell lysates were extracted by RIPA lysis buffer (Thermo Scientific, Cat#8901) in the presence of 1×Phosphatase Inhibitor [Complete Mini EDTA-free medium; Roche, Cat#4693132001], 1×PMSF (CST, Cat#8553S) on ice and sonicated using a Biorupter (Advanced-High mode, 30s ON/30s OFF, 10 cycles). After collecting the lysates supernatant by centrifugation (12,000×g, 10min, 4 °C), protein concentration was determined using a BCA Protein Assay Kit (Thermo Scientific, Cat#23227). Equal amounts of protein were loaded per lane on 4–12% SDS-PAGE gels to perform the migration step. Note that samples were not boiled prior to SDS-PAGE when analysing membrane proteins and mitochondrial-encoded proteins. Subsequently proteins were transferred to 0.2μm or 0.45μm nitrocellulose membranes (Cytiva, Cat#10600015 or Cat#10600023). Ponceau S staining (Sigma, P7170) for total protein was commonly used for detecting transfer efficiency. After blocking with 5% (w/v) fat-free milk in Tris-buffered saline with 0.1% Tween 20 detergent (TBST) for 1h at room temperature (RT), membranes were immediately incubated with corresponding primary antibodies overnight at 4 °C to probe their respective targets. The next day, the membranes were incubated with horseradish peroxidase-conjugated secondary rabbit or mouse antibody (Bio-RAD, Cat#170–6515, Cat#170-6516) at RT for 1 h. After adding ECL substrates (Bio-RAD, Cat#170–5061), the blots were then visualized on LAS-4000 (FUJIFILM) or Vilber Chemiluminescence system (Vilber). Protein expression levels were quantified by densitometric analysis with Image J software (NIH).

The following antibodies and corresponding dilution ratios for Immunoblotting used in this study: Anti-β-actin (Sigma, A5441, 1:5000); Anti-Cleaved-Caspase3 (CST, Cat#9662, 1:1000); Anti-Phospho-Histone H2A.X (CST, Cat#9718T, 1:1000); Anti-Cleaved-PARP (CST, Cat#9546S, 1:1000); Anti-COX2 or MT-CO2 (abcam, ab110258, 1:1000); Anti-MDR1 or P-Glycoprotein or ABCB1 (abcam, ab170904, 1:2000); Goat Anti-Rabbit IgG (H+L)-HRP (Bio-Rad, Cat#1706515, 1:5000); Goat Anti-Mouse IgG (H+L)-HRP (Bio-Rad, Cat#1706516, 1:5000).

Measurement of intracellular lipid droplets (LDs) content

Bodipy 493/503 fluorescent dye (Invitrogen, D3922), which binds intracellular neutral lipids, was utilized to evaluate LDs content in vitro. Cells were washed with 1×PBS once and spun onto glass slides by using Cytospin-4 (Epredia™, A78300003), followed by fixation with 4% Paraformaldehyde (EMS, Cat#157-4) for 20min at RT and two washing steps with 1×PBS. Stained cells with

Bodipy 493/503 working solution (1μM) for 30 min at 37 °C in dark. After washing twice with 1×PBS, labeled cells were proceeded to nuclear counterstain with Hoechst (2μg/mL, Invitrogen, H3570) for 20 min. Subsequently, the cells were washed three times with 1×PBS before final mounting of the coverslips on a glass slide using Fluorescence Mounting Medium (Dako, S3023). The fluorescence images were captured using a fluorescence microscope (Axio Imager 2_apotome; ZEISS) with 63× objective (oil-immersion).

For FACS test, experiment setup and data acquisition were using Attune™ NxT Flow Cytometer and Attune™ NxT Software rev 3.1.2. Fluorochrome was excited with a 488nm laser (BL1 signal). Bodipy 493/503 signal of each sample was displayed as a histogram.

RNA-seq data processing

Total RNA was isolated and purified using AllPrep DNA/RNA/Protein Mini Kit (QIAGEN, 80004). The quantity and integrity of RNA was assessed using the Agilent 2100 bioanalyzer. Total RNA-seq libraries were prepared using the KAPA RNA HyperPrep kit (Roche, 07962312001) and subsequently sequenced on the NovaSeq 6000 platform (Illumina) following the manufacturer's protocol. Reads were aligned using the STAR software [13] and counted using HTSeq framework [14]. From the read counts RPKM (Reads Per Kilobase Million) values were calculated and then log-transformed by taking log2 (1 + RPKM). Due to potentially high and cell-type-specific copy numbers of mtDNA, the RPKM data normalization was performed using nuclear DNA coverage to ensure accurate mitochondrial gene expression estimation.

Batch effect correction and sensitivity analyses in RNA-seq data

The batch effect between two original RNA-seq datasets of T-ALL patients was corrected using the Python package "pyComBat 0.3.3" [15]. To assess the impact of this correction, we performed several sensitivity analyses, presented in Suppl. Fig. S1 and S9. First, we conducted Principal Component Analysis (PCA) before and after batch correction using the total transcriptome from the initial T-ALL datasets. Prior to pyComBat correction, the two datasets formed distinct clusters due to batch effects. After correction, this separation disappeared (Supp. Fig. S1A).

Next, we evaluated expression level distributions before and after batch correction for key genes in our analysis: *ACTB* (beta-actin) as a control and *ABCB1* as the primary gene of interest. We observed a strong correlation (Pearson correlation coefficient > 0.9) between pre- and post-correction expression levels in both cases (Supp. Fig. S1B). Additionally, we computed Pearson correlation coefficients across the entire transcriptome before and after batch correction. The results showed a strong correlation for nearly all genes (Supp. Fig. S1C), indicating that the pyComBat correction did not alter the biological findings.

To further validate the robustness of our results, we compared key findings with and without batch correction. Specifically, we analyzed *ABCB1* expression levels separately in the initial uncorrected datasets and in the pooled dataset after batch correction (Supp. Fig. S1D). We also generated survival curves for the ABCB1- and ABCB1+ groups (Supp. Fig. S1E). In both cases, the trends observed in the original datasets remained consistent with those in the final pooled dataset after correction. While p-values in the original datasets were sometimes significant and sometimes not due to smaller sample sizes, pooling the datasets substantially increased statistical power, leading to consistently significant p-values.

Furthermore, we successfully reproduced the key results from our Gene Set Enrichment Analysis (GSEA) both in the individual uncorrected datasets and in the pooled dataset after pyComBat correction (Supp. Fig. S9). In all cases, the results remained highly similar and statistically significant, confirming that the pyComBat correction did not distort the underlying biological signals in our transcriptomic data.

Statistical analysis

Statistical analysis was carried out using GraphPad Prism version 8, R version v4.2.3 and Python version 3.11. Two-tailed unpaired Student's t test was utilized to compare between two groups. Statistical difference was noted as significant if $p < 0.05$. *$p < 0.05$; **$p < 0.01$; ***$p < 0.001$; ****$p < 0.0001$; ns, no significant. For survival outcomes, overall survival (OS) was calculated as the time from the date of diagnosis to the date of death or last follow-up (censored). Survival analysis was performed using the log-rank statistical test.

Gene set enrichment analysis (GSEA)

The Gene Set Enrichment Analysis (GSEA) was carried out on a selection of gene sets related to mitochondria function and lipid metabolism from two public databases made available by the Broad Institute: MSigDB (https://www.gsea-msigdb.org/gsea/msigdb/) and MitoPathways3.0 [16] (https://www.broadinstitute.org/mitocarta/mitocarta30-inventory-mammalian-mitochondrial-proteins-and-pathways) [17–19]. The GSEA analysis was performed using the Python package "gseapy" [20].

Identification of the groups having high (MT+) or low (MT-) mitochondrial electron transport chain (ETC) activities in RNA-seq data

To identify the groups of high (MT+) and low (MT-) of mitochondrial ETC activity, we used the transcriptomic data of 161 genes, identified in the gene set "GOBP ELECTRON TRANSPORT CHAIN" of the database MSigDB and available in our pooled adult T-ALL dataset. First, we calculated z-scores for these genes based on their normalized expression levels by subtracting the mean expression value and dividing the result by the standard deviation. We then averaged the z-scores for each T-ALL sample. Finally, we selected the 20% of samples (n = 26) with the lowest average z-scores as the MT- group and the 20% with the highest average z-scores as the MT+ group (Fig. 1A).

Resources

The sources of all the cell lines, antibodies and reagents used in this study can be found in the supplementary file: key resource tables.

Results

Characterization of the impact of the mitochondrial activity on the biology of adult T-ALL

In order to increase our statistical power in the transcriptomic analysis of adult T-ALL, we have generated bulk transcriptomic data of 79 additional samples from Ruijin hospital adult T-ALL patients. Data from this new cohort added to the previously published 54 tumour samples [7], allows us to dispose of the largest known T-ALL cohort transcriptomic data, encompassing 133 tumours with median follow-up of 32 (95% confidence interval [CI], 25.348–38.652) months. The summarized clinical characteristics of these patients are detailed in the following Table 1. Among this Chinese ethnic population with T-ALL, 91 cases were male and 42 cases were female, male (M): female (F) = 2.17: 1. The median age was 33 years (IQR, 22.5–47.5), median percentage of leukemia cell blasts in bone marrow at the initial presentation (blasts %) was 88.1% (IQR, 76–92.5%), median first-episode white blood cell (WBC) count was 25.77 (IQR, 6.2–94.245) $\times 10^9$/L, median hemoglobin (HB) concentration was 106 (IQR, 80–133) g/dL, median platelet (PLT) count was 91 (IQR, 42–168) $\times 10^9$/L. The results of classification based on immunophenotype were Pro-50 (37.59%), Pre-42 (31.58%), Cortical-32 (24.06%), and Medullary-9 (6.77%) cases; and 54 (40.60%), 8 (6.02%) and 71 (53.38%) cases were categorized as ETP, near-ETP and non-ETP subtype, respectively. The NOTCH1 mutation rate in this cohort was 64.66%. Of the 108 patients for whom karyotype analysis data were available, 22 patients carried more than 3 cytogenetic abnormalities (abn). 15 (11.28%) patients had central nervous system (CNS) involvement, i.e., meningeal leukemia, at the time of initial diagnosis or during the course of treatment (Table 1).

All patients underwent induction chemotherapy with the VDPCP regimen, and 62 (46.62%) patients successfully bridged to hematopoietic stem cell transplantation (HSCT) procedure. Initial clinical outcome analysis of the above 133 adult T-ALL patients showed a complete remission (CR) rate of 84.87% at any time point in evaluable patients (n = 119), with morphologic relapse present in 29 (28.71%) patients at a later stage. Additionally, 73 (54.89%) patients experienced progression during the course of treatment (Table 1).

First, we fused the two datasets and removed the batch effect with the "pyComBat" software (Python package "pyComBat" version 0.3.3). Principal Component Analysis (PCA) analysis of the pooled population showed an effective merging of the two populations and the creation of a homogenous sets of transcriptomic data (Fig. S1A).

We then used the transcriptome signature "GOBP ELECTRON TRANSPORT CHAIN" from the MSigDB database, encompassing all nuclear genes encoding components of electron transport chain (ETC) complexes [21], to identify samples with high (MT+) and low (MT-) mitochondrial ETC activities (Fig. 1A), as described in the Materials and Methods section.

We then specifically focussed on genes differentially expressed between the two selected populations "MT+" versus "MT-" (Fig. 1B, C), and performed the Gene Set Enrichment Analysis (GSEA) to characterise the most affected cellular processes in tumours with lower mitochondrial activity. The detailed results of the differential analysis are available in Supp. Table 1.

GSEA results pointed to significant depletion of genes encoding factors involved in mitochondrial lipid metabolism, more specially β-oxidation in the MT- population (Fig. 2A).

Additionally, we examined the expression of glycolytic genes in MT- tumours. Surprisingly, our analysis revealed that most tumours with dysfunctional mitochondria also exhibit a depleted glycolytic gene expression signature (Fig. 2B). The metabolic profile of these tumours reminded us of the work by Herranz D and colleagues, which described a metabolic shutdown in a specific subset of T-ALL tumours [22]. This study reported that autophagy was activated as a salvage pathway to support leukemia cell metabolism. Interestingly, we also found that MT- tumours exhibit an enriched autophagy gene signature (Fig. 2C). These findings suggest that MT- tumours share key metabolic characteristics with the previously described aggressive T-ALL tumours [22].

Since our previous research pointed that low mitochondrial activity was associated with MRD+ patients

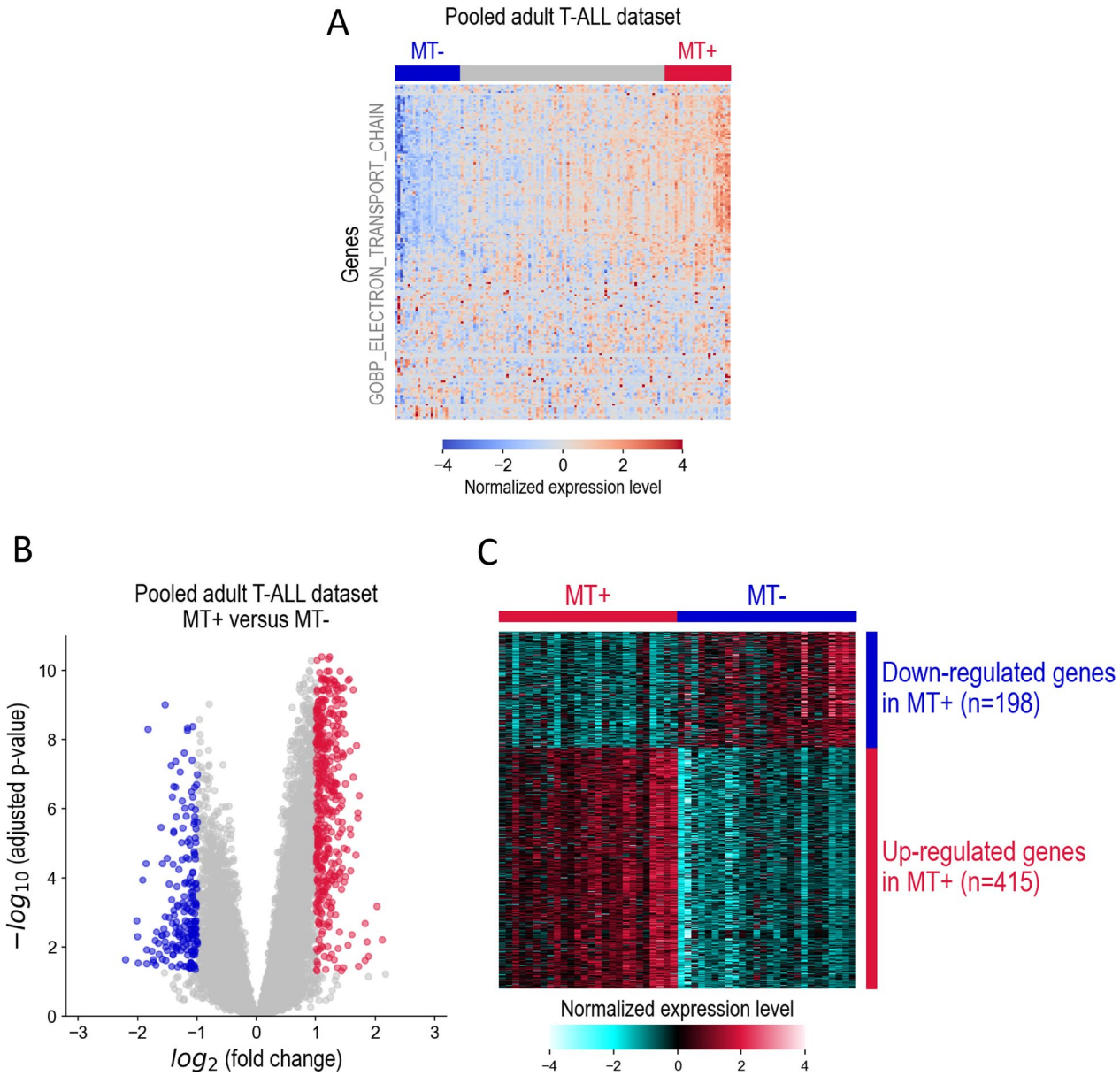

Fig. 1 Identification of the mitochondrial depleted adult T-ALL tumours. **A**: Heatmap of normalized expression levels in our pooled adult T-ALL dataset, for 161 genes available in the human gene set "GOBP ELECTRON TRANSPORT CHAIN" (database MSigDB, collection C5: "Ontology/Gene Ontology/Biological Process"). The T-ALL samples are ordered accordingly to the average normalized expression level across the 161 genes. The group "MT-", shown in blue, corresponds to 20% of T-ALL samples (n = 26) with low expression levels of these genes. The group "MT+", shown in red, corresponds to 20% of T-ALL samples (n = 26) with high expression levels. The expression levels were normalized using the z-scores. **B**: Volcano plot showing the results of the differential analysis performed in the group "MT+" versus the group "MT-". The x-axis represents the log2 value of the fold change calculated between the average expression levels in the groups "MT+" and "MT-". The y-axis shows the -log10 of the adjusted p-value obtained with the two-sided t-test between the distributions of expression levels in the groups "MT+" and "MT-". Significantly down-regulated genes in the group "MT+" versus the group "MT-" are plotted in blue dots. Significantly up-regulated genes are shown in red dots. We considered that the expression levels between the groups "MT+" and "MT-" were significantly different if the adjusted p-value < 0.05 and the absolute value of the fold change > 2. The detailed results of the differential analysis are available in Supp. Table S1. **C**: Heatmap of the differential expression profiles of the "MT+" group versus the "MT-" group in the pooled adult T-ALL dataset, with the differentially expressed genes presented in Fig. 1B. The hierarchical clustering was performed using Euclidian-based distance with Ward's linkage for samples and Pearson correlation for genes

[8], we analyzed our GSEA results to understand why these cells resist treatment. Given that *ABCB1* is a well-known drug resistance gene, we focused on the ABC transporter gene set—particularly the *ABCB1* member. Indeed, our GSEA data revealed a significant enrichment of ABC transporters encoding genes expression in the MT- tumours (Fig. 2D). Among the ABC transporters gene family, *ABCB1*, known also as multidrug resistance factor 1 (MDR1), encoding P-glycoprotein (P-gp) stands out. Indeed, this protein mediating the efflux of drugs out of the cells, could significantly impact tumour cells' drug responses and resistance to treatment [23]. We specifically considered the differential expression of *ABCB1* between the MT+ and MT- populations and found that the gene is significantly upregulated in the MT- tumours (Fig. 2E).

Down-regulation of mitochondrial activity mediates the activation of *ABCB1*

Taking into account the inverse relationship between mitochondrial activity and *ABCB1* gene activation, we decided to use T-ALL model cell lines and consider *ABCB1* mRNA accumulation following the depletion of their mitochondria. First, using a qPCR screening for mitochondrial DNA, of several model T-ALL cell lines, we showed that except the SUP-T1 cells, all the considered cell lines bear a relatively comparable number of mitochondrial genomes per cell (Fig. S2). We then choose CCEF-CEM and MOLT-4 cell lines for further investigations. Treatment of cells with low dose of Ethidium Bromide (EtBr) for several days is known to specifically interfere with mitochondrial DNA replication, leading to a decrease in mitochondria number following successive cell division cycles [24]. In our case, a significant depletion in mitochondria was observed after about 7 days treatment in both cell lines (Fig. S3A), accompanied by a decrease in the amount of COX2 (Cytochrome C Oxidase subunit 2), which is encoded by the mitochondrial genome (Fig. S3B).

The critical question was then to know if the induced decrease in cell mitochondria would induce in turn the activation of *ABCB1* gene.

Immunoblotting revealed a considerable accumulation of P-gp in EtBr-treated MOLT-4 cells and CCRF-CEM cells (Fig. 3A). To make sure that mitochondrial activity, and not an indirect effect of EtBr treatment, was involved in the induction of *ABCB1* expression, we have also treated these cells with an unrelated molecule, Chloramphenicol (CAP), inhibiting the synthesis of mitochondrial proteins [24]. CAP treatment also significantly induced P-gp in CCRF-CEM, cells but not in MOLT-4 cells (Figs. S4A and S4B). Interestingly, the inability of MOLT-4 cells to induce *ABCB1* gene was correlated with the inability of CAP to mediate a decrease in COX2 (Fig. S4B), showing that in these cells, CAP is not an effective drug for inhibiting mitochondrial protein translation. We also tested another cell line JURKAT, which also presented an increased P-gp protein accumulation upon CAP treatment and a decrease in mitochondrial protein synthesis (Fig. S4C). These data show that mitochondrial DNA depletion or the inhibition of mitochondrial translation are directly linked to the induced expression of *ABCB1*.

Taking into account the more effective cell response to EtBr treatment, we used this treatment for our following functional experiments.

The GSEA analysis revealed that tumour cells with reduced mitochondria ETC activity also present a reduced mitochondria fat lipid metabolism and more specifically, an impaired β-oxidation (Fig. 2A). We reasoned that cells with low mitochondrial activity, which maintain continuous de novo lipid synthesis (DNL), should also accumulate neosynthesized fat molecules in the form of lipid droplets [25].

To test this hypothesis, we directly measured lipid accumulation in our two model cell lines using lipid-specific dye, Bodipy. Figure 3B shows that in both cell lines, mitochondria depletion led to a significant accumulation of lipid droplets, visible both by microscopy and by FACS.

(See figure on next page.)

Fig. 2 Biological features of mitochondria are depleted in adult T-ALL tumours. **A**: Results of the GSEA analysis for the gene set of fatty acid β-oxidation from the database MSigDB and for the gene set of lipid metabolism from the database MitoPathways, calculated in the T-ALL group "MT+" versus the group "MT-" of our pooled adult T-ALL dataset. The GSEA results were considered significant if the calculated p-values < 0.05 and false discovery rates (FDR) < 0.25. Mitochondria-depleted T-ALL tumours "MT-" are significantly depleted for lipid metabolism and β-oxidation. **B**: Results of the GSEA analysis for three gene sets of glycolysis from the database MSigDB. These gene sets are significantly enriched in the group "MT+" compared to the group "MT-". **C**: Results of the GSEA analysis for the gene set "GOBP POSITIVE REGULATION OF AUTOPHAGY" which is significantly depleted in the in the group "MT+" versus the group "MT-". **D**: Results of the GSEA analysis for the gene set of ABC transporters, calculated in the T-ALL group "MT+" versus the group "MT-". Mitochondria-depleted T-ALL tumours "MT-" are significantly enriched for genes expressing the ABC transporter family. **E**: Comparative expression levels of the gene *ABCB1* in the groups "MT+" and "MT-". The expression levels of *ABCB1* are significantly higher in mitochondria-depleted T-ALL tumours. The p-value corresponds to the two-sided statistical t-test. Additionally, the figure indicates the corresponding effect size (Cohen's d) and 95% confidence interval

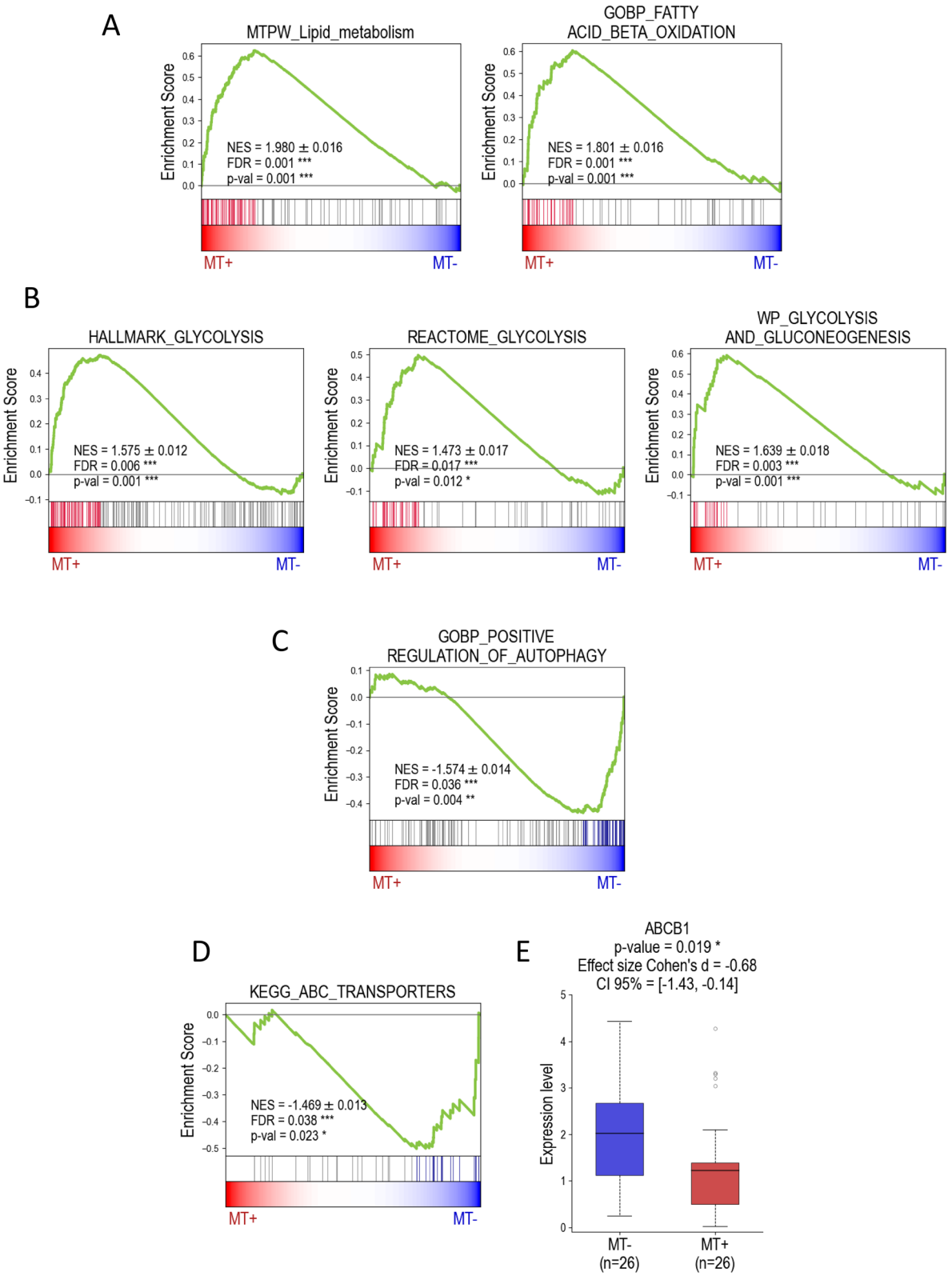

Fig. 2 (See legend on previous page.)

De novo lipid synthesis and accumulation mediate *ABCB1* activation

Since β-oxidation impairment in tumours with low mitochondrial activity and in mitochondria depleted T-ALL cell lines could favour lipid accumulation, we wondered whether lipid accumulation and the DNL—fed intermediary lipid products could be at the origin of *ABCB1* gene activation. To answer this question, after mitochondrial depletion and the activation of *ABCB1* gene, cells were treated with ND-630, a specific inhibitor of acetyl-CoA carboxylase 1 (ACC1), the first enzyme of DNL. Interestingly, treatment of cells with either 100nM or 1μM of ND-630 completely abolished the *ABCB1* gene activation in mitochondria-depleted cells (Fig. 4A). We also tested whether de novo synthesized fatty acids products, dietary medium chain saturated fatty acid, octanoate, could also induce *ABCB1* gene activation. In control CCRF-CEM, as well as in MOLT-4 cells, octanoate treatment had no effect on *ABCB1* gene expression, but could remarkably enhance *ABCB1* gene expression in mitochondria-depleted cells (Fig. 4B).

Since octanoate was effective in activating the *ABCB1* gene only after mitochondrial depletion, we wondered whether octanoate degradation via β-oxidation would be the reason why octanoate did not induce *ABCB1* gene expression in our control EtBr-untreated T-ALL cells.

To test this hypothesis, we treated control CCRF-CEM and MOLT-4 cells with the FDA approved partial inhibitor of β-oxidation, Ranolazine. Interestingly, in both cell lines, the treatment of control cells with active mitochondria with both octanoate and Ranolazine, significantly induced *ABCB1* gene expression, without a need for mitochondrial depletion (Fig. 4C). These data highlighted one of the important mechanisms involved in *ABCB1* gene activation that depends on the down regulation of fatty acids β-oxidation. Octanoate is mostly degraded by β-oxidation [26] and the inhibition of β-oxidation even partially, makes it available to induce *ABCB1* gene activity.

These data clearly show that in the absence of mitochondria and lipid β-oxidation, lipid neo synthesis and accumulating lipids are the major drivers of *ABCB1* gene activation (Fig. 4D).

Lipogenic transcription factors, LXRs, are the major drivers of *ABCB1* gene activation

Since DNL and more specifically the DNL intermediary product and a dietary fat, octanoate efficiently induce *ABCB1* gene expression, we wondered if octanoate itself could be an activator of a specific transcription factors inducing *ABCB1* gene expression. A search of the literature for transcription factors that could be activated by octanoate pointed to the work of Bedi and colleagues who demonstrated that medium-chain saturated fatty acids, namely octanoate, in contrast to longer-chain fatty acids, binds to LXRα with an affinity in the nanomolar range and activates this transcription factor [27]. These data prompted us to consider LXR factors as prime candidates in mediating the lipid-dependent activation of *ABCB1*. Luckily, specific and efficient agonist and antagonist of LXR are available, which enabled us to test our hypothesis on the role of LXR in the lipid-mediated activation of *ABCB1*. Interestingly, in control CCRF-CEM and MOLT-4 cells, LXR agonist GW3965 efficiently induced *ABCB1* gene activation, even in the presence of mitochondria (Fig. 5A, left panels). In mitochondria-depleted cells, GW3965 also further enhanced *ABCB1* activation (Fig. 5A, right panels). These data clearly show that the lipogenic transcription factors LXRs are major player in *ABCB1* gene transcription activation. To confirm the involvement of LXR transcription factors in the mitochondria depletion-dependent activation of *ABCB1*, CCRF-CEM and MOLT-4 were treated with EtBr to deplete mitochondria and then treated with the LXR antagonist GSK2033. Figure 5B shows that in both cell lines, the activated *ABCB1* gene expression was down-regulated by treatment of cells with the LXR antagonist, GSK2033.

Finally, to further confirm the activation of LXR transcription factors in MT- tumours, we analyzed our adult T-ALL transcriptomic data to assess the expression of well-characterized LXR target genes. A review of the literature identified *ABCA1*, *ABCG1*, *ABCG5*, and *ABCG8* as key targets of LXR transcription factors [28, 29]. We performed a t-test to compare the expression levels of these genes between MT+ and MT- tumours. Notably, *ABCG5* and *ABCG8* were not

(See figure on next page.)

Fig. 3 Mitochondria depletion induces P-gp protein accumulation with a concomitant lipid accumulation. **A**: CCRF-CEM and MOLT-4 cells were treated with 200ng/mL and 100ng/mL Ethidum Bromide (EtBr), respectively, for 7 days, proteins were extracted and P-gp accumulation was visualized by immunoblotting. Immunodetection of β-actin demonstrated the state of protein loading (left panel). The quantitative analysis of P-gp protein expression levels was visualized as histograms (right panel) (n = 3, mean ± SEM; difference compared to the control group were calculated by two-tailed unpaired Student's t test). ***p < 0.001; ****p < 0.0001. **B**: CCRF-CEM and MOLT-4 cells were treated with 200ng/mL and 100ng/mL Ethidium Bromide (EtBr) for 7 days, respectively, as described in (A) and cells were stained by Bodipy 493/503 and examined by FACS (upper panels) and by fluorescence microscopy (lower panels, scale bar = 10μm). The fluorescence intensity of unstained and stained non-treated and treaded cells measured by FACS are indicated (X axis) (middle panels). Error bars indicate SEM. *p < 0.05; **p < 0.01

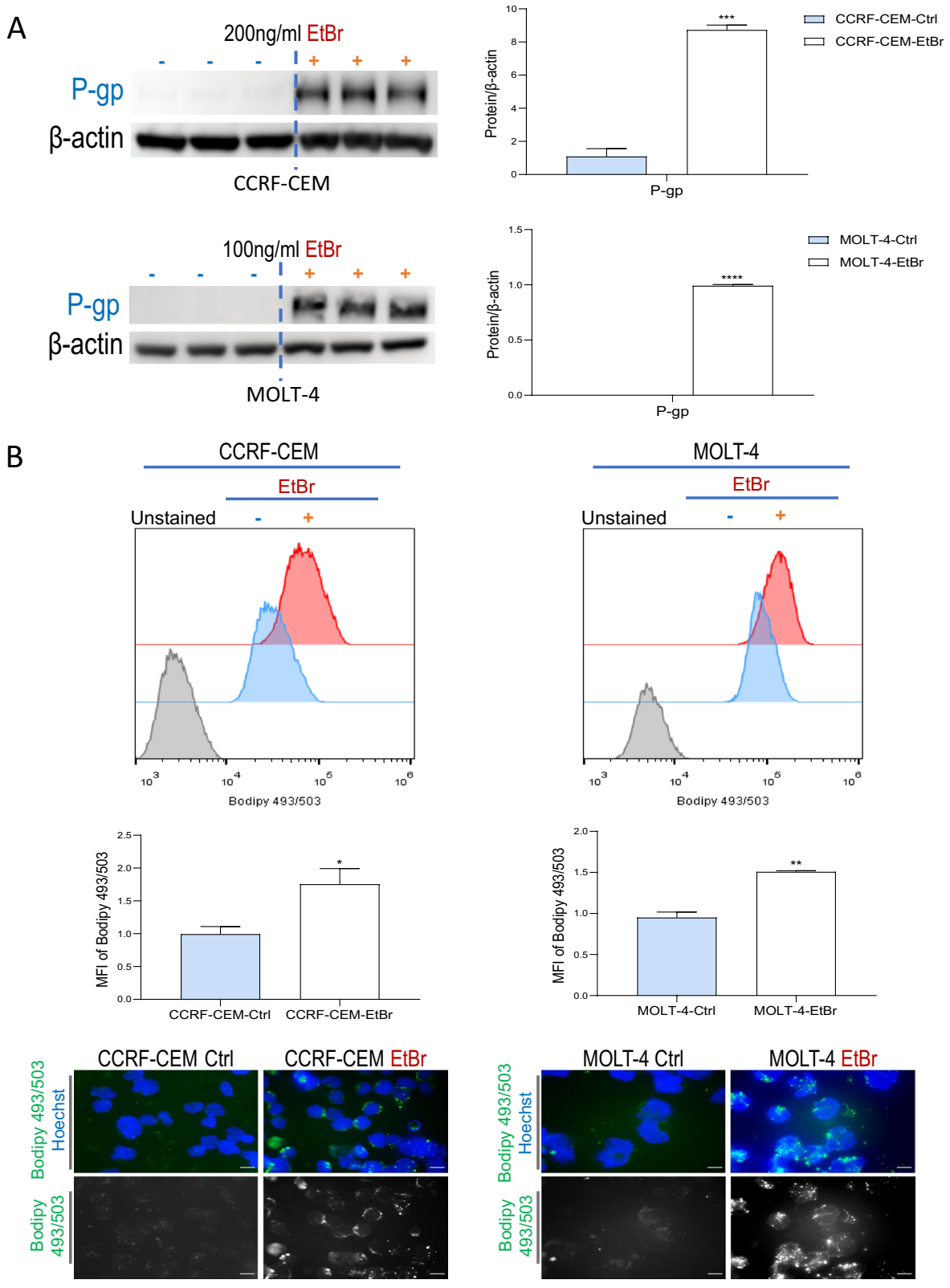

Fig. 3 (See legend on previous page.)

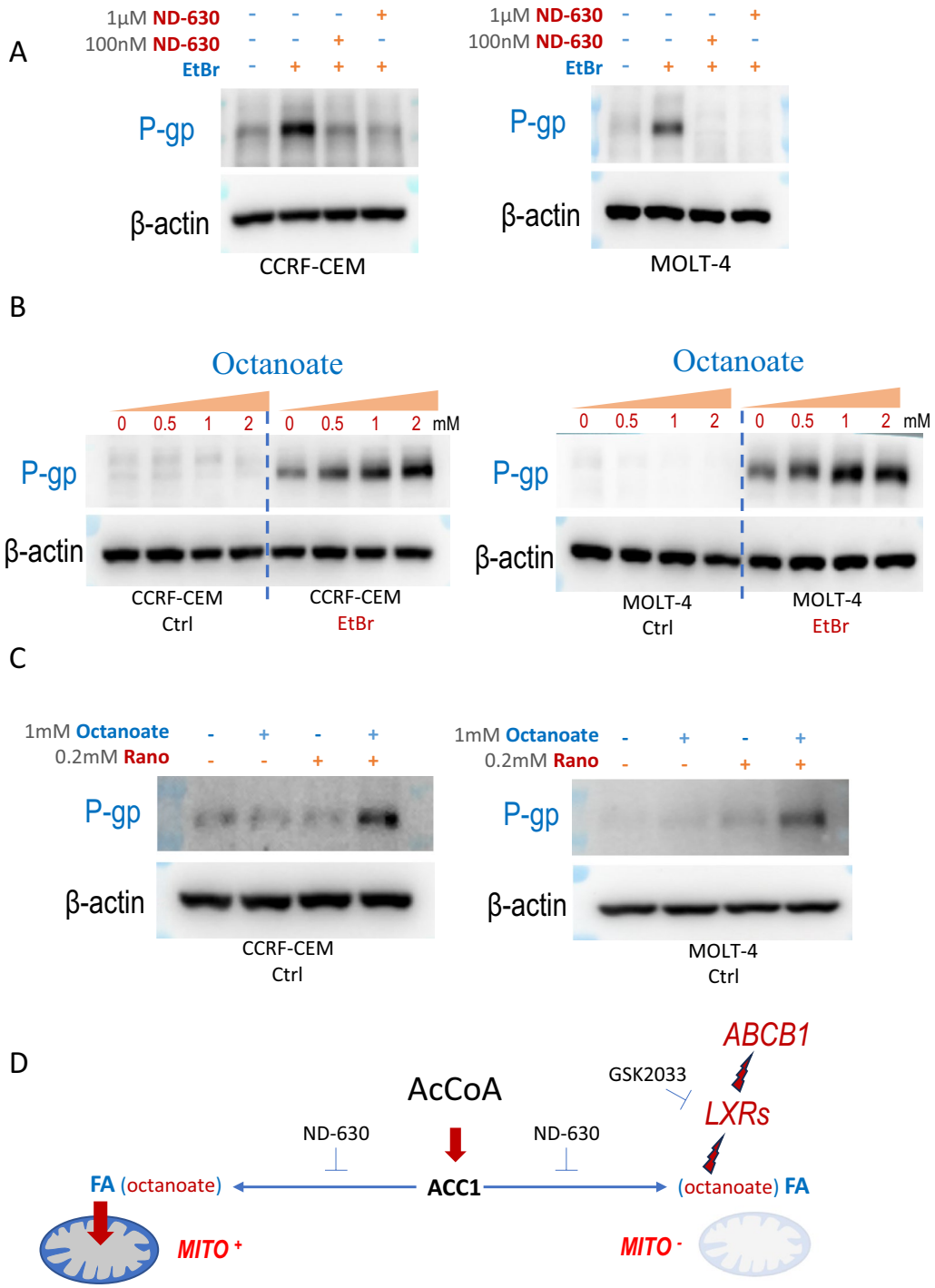

Fig. 4 De novo lipogenesis and octanoate mediate the activation of *ABCB1* gene. **A**: Control or Ethidium Bromide treated (200ng/mL and 100ng/mL, respectively) CCRF-CEM and MOLT-4 cells were treated with the ACC1 inhibitor, ND-630, with the indicated concentration for 7 days and P-gp and β-actin accumulation visualized by immunoblotting. **B**: Control or Ethidium Bromide treated (200ng/mL and 100ng/mL, respectively, for 7 days) CCRF-CEM and MOLT-4 cells were treated with the indicated concentrations of octanoate for 24 h and the accumulation of P-gp and β-actin accumulation was visualized as above. **C**: Control CCRF-CEM and MOLT-4 cells were treated concomitantly with the indicated concentration of octanoate and the partial β-oxidation inhibitor, Ranolazine, and the accumulation of P-gp and β-actin accumulation was visualized as above. **D**: The scheme illustrates the following hypothesis: In cells with normal mitochondrial activity, DNL products and octanoate are degraded by the mitochondrial β-oxidation and therefore they would not be available to induce *ABCB1* gene expression (left). In mitochondria-depleted cells, DNL products and octanoate are available and mediate the induction of *ABCB1* gene

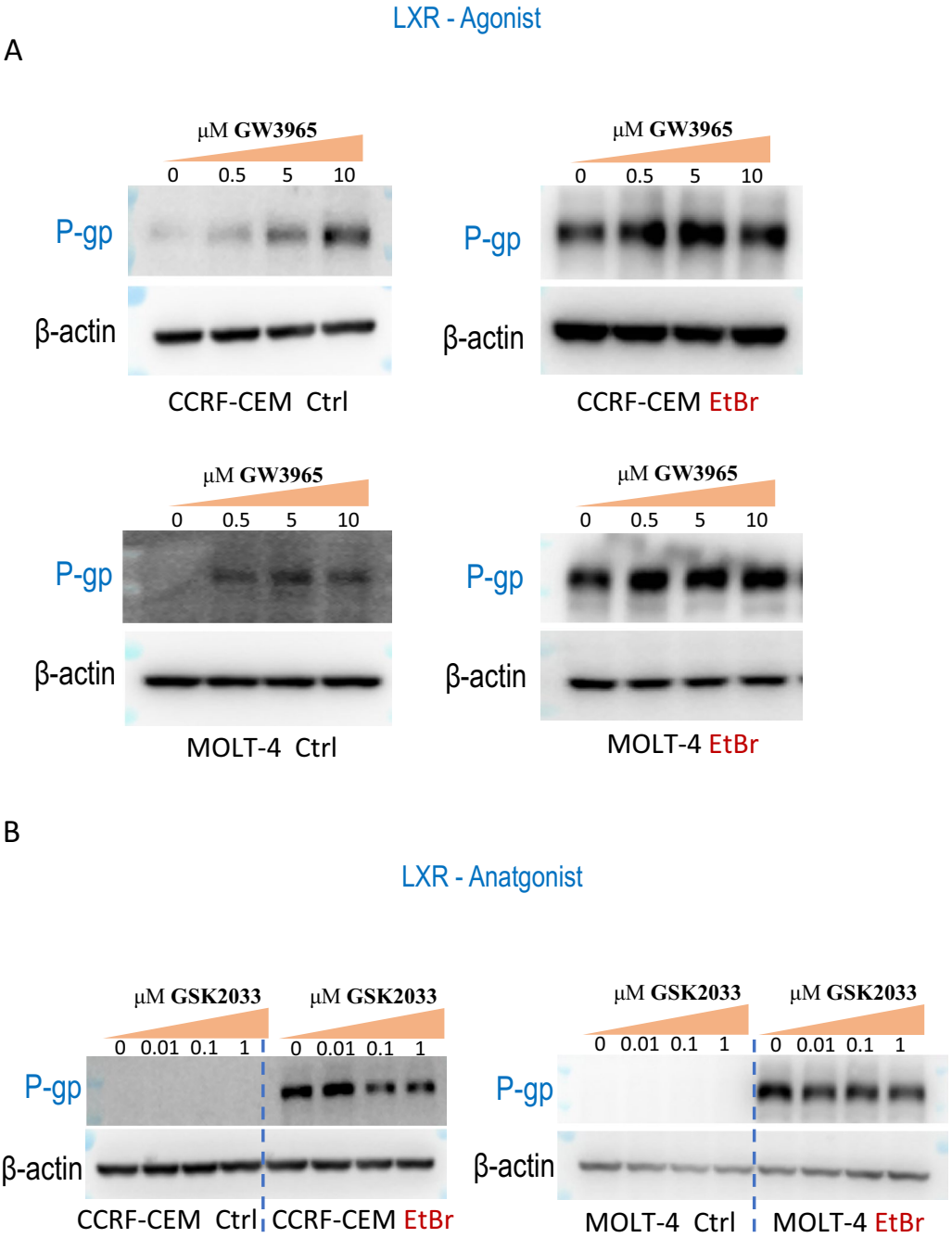

Fig. 5 Lipogenic transcription factors LXR mediate the lipid-dependent activation of *ABCB1* gene. **A**: Control (left panels) or Ethidium Bromide treated (200ng/mL and 100ng/mL, respectively, for 7 days) (right panels) CCRF-CEM and MOLT-4 cells (indicted), were treated with the indicated concentrations of LXR agonist, GW3965, for 24 h and the accumulation of P-gp and β-actin was visualized as above. **B**: The same experiment as above was carried out expect that cells were treated with LXR antagonist GSK2033, with the indicated concentration for 24 h

detected in our tumour transcriptome. The most striking findings were for *ABCA1*, a well-established LXR target, and potentially *ABCG1*, which showed near-significant results (Fig. S5A). Furthermore, we also tested the relationship between β-oxidation shutdown and LXR gene activity in our T-ALL transcriptome as follows. We first considered the 27 leading-edge genes out of 76 genes in the "GOBP FATTY ACID BETA OXIDATION" gene set signature (Fig. S5B).

Then, we went back to our adult T-ALL transcriptome and considered samples with "Fatty-Acid-Beta-Oxidation positive" and "negative" To avoid the confusion with the previous groups (MT- and MT+), we named the "Fatty-Acid-Beta-Oxidation positive" and "negative" groups LEG-FABO+ and LEG-FABO- (Fig. S5C). Finally, we calculated the distributions of expression levels in these groups for *ABCA1*, which is a well-characterized target of LXRs. This analysis revealed that the depletion of key genes encoding β-oxidation enzymes triggers the activation of *ABCA1*, providing clear evidence of LXR activation in "Fatty-Acid-Beta-Oxidation negative" tumors (Fig. S5D).

These data strongly support the model where de novo lipogenesis or dietary fats such as octanoate and the absence of fatty acids degradation by β-oxidation, activate LXR transcription factors that in turn activate *ABCB1* gene expression.

Lipid accumulation, down-regulation of OXPHOS and β-oxidation drive *ABCB1* gene activation in adult T-ALL tumour samples

In order to confirm our findings on the driver role of mitochondria depletion in *ABCB1* gene activation, we decided to follow an unbiased approach considering the differential gene expression in adult T-ALL tumour samples expressing the highest levels of *ABCB1* (ABCB1+) versus tumours expressing low levels of this gene (ABCB1-). The groups ABCB1+ and ABCB1- were separated using the median expression level of *ABCB1* as a threshold. The detailed results of the differential analysis are available in Supp. Table S2.

We found that tumours expressing high levels of *ABCB1* also activate and down-regulate 139 and 89 genes respectively (Fig. 6A). Interestingly, GSEA confirmed that high expression of *ABCB1* is associated with a considerable depletion of mitochondrial gene module and electron transport chain-encoding genes (Fig. 6B, Fig. S6). More interestingly, as expected from our experiments, the high *ABCB1*-expressing tumours are also enriched for lipid droplet function (Fig. 6C).

These data therefore strongly support the molecular mechanisms underlying tumour aggressivity and resistance to induction treatment associated with deficient mitochondrial activity.

Impaired mitochondrial activity and the absence of β-oxidation favours the accumulation of neosynthesized fat through DNL and the accumulation of intermediary fatty acids, which activate the lipogenic LXR transcription factors, which in turn activate *ABCB1* gene conferring resistance to induction chemotherapy.

To confirm and highlight the impact of high *ABCB1* expression on tumour aggressivity, we could demonstrate a significantly shorter survival of patients with high expression of *ABCB1* (Fig. 7). Additionally, using our model cell lines we could also show that the depletion of mitochondria is associated with a significantly increased resistance to drug used in first-line chemotherapy (Fig. S7). To further show that mitochondria depletion and the subsequent LXR transcription factor activation is driving this observed resistance, we repeated the experiment described above also in the presence of LXR antagonist, GSK2033. Figure S8A, B clearly shows that in both model cell lines inhibition of LXR activity leads to an increased sensibility to the drug used in conventional chemotherapy. Since LXR transcription factors induce the expression of several ABC transporters, we repeated this experiment in the presence of the MDR1 inhibitor, Tariquidar [30], to assess the significant contribution of *ABCB1* to the observed resistance to conventional chemotherapy. Notably, inhibiting MDR1 activity significantly increased the sensitivity of our model cells to the applied chemotherapy (Fig. S8C, D).

Discussions

Previously, we found that the mitochondrial gene module is globally depleted in MRD-positive T-ALL tumours, as well as in aggressive tumours (irrespective of their MRD status), identified using our gene expression classifier signature [8]. Thanks to the increased statistical power provided by the addition of the whole transcriptome of 79 new adult T-ALL samples, we were able to highlight the main biological characteristics of adult T-ALL tumours with depleted mitochondria.

As a result of this analysis, we noticed that, in addition to the expected depletion of mitochondrial functions

(See figure on next page.)

Fig. 6 Biological features of adult T-ALL tumours expressing high levels of *ABCB1*. **A**: Results of the differential analysis between two groups of T-ALL patients with low expression of the gene *ABCB1* (group "ABCB1-", n = 67) and high expression of the gene ABCB1 (group "ABCB1+", n = 66). The groups of low and high expression were identified with respect to the median expression level of *ABCB1* in the total pooled adult T-ALL dataset. The volcano plot (left) and heatmap (right) were calculated similarly to Fig. 1B. The detailed results of the differential analysis are available in Supp. Table S2. **B**, **C**: Results of the GSEA analysis in the group "ABCB1+" versus the group "ABCB1-". T-ALL tumours expressing high levels of *ABCB1* are significantly depleted for gene expression involved in mitochondria function (**B**) and significantly enriched for gene expression involved in lipid droplet formation (**C**). The GSEA results were considered significant if the calculated p-values < 0.05 and false discovery rates (FDR) < 0.25

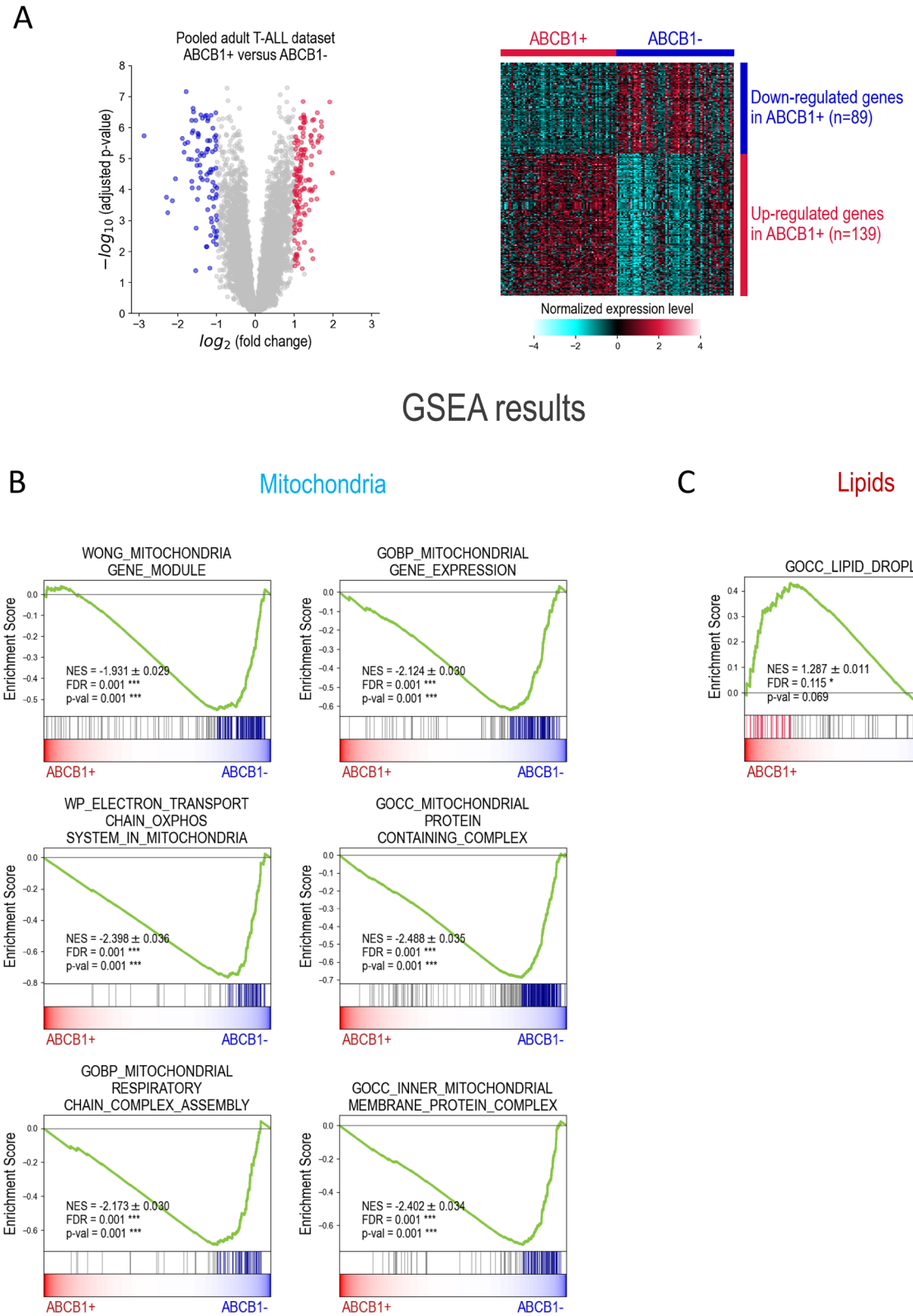

Fig. 6 (See legend on previous page.)

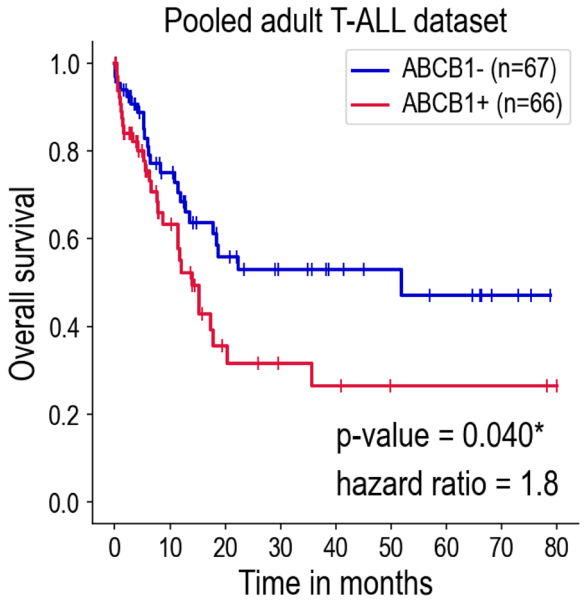

Fig. 7 Poor prognosis of T-ALL tumours expressing high levels of *ABCB1*. Kaplan-Meier survival curves in the groups of patients with low level of *ABCB1* expression (group "ABCB1-"), shown in blue line, and high level of *ABCB1* expression (group "ABCB1+"), shown in red line, in the pooled adult T-ALL dataset. *ABCB1* expression groups were determined using the median expression level as a threshold. The p-value and hazard ratio were calculated using the log-rank test

such as lipid β-oxidation, there was a significant up-regulation of genes encoding the ABC transporters. This observation provided an obvious explanation as to why the impairment of mitochondrial activity could be associated with overt resistance to drug treatment. Indeed, several members of the ABC transporter, in particular the well-known drug resistance factor, MDR1 (P-gp protein), encoded by the *ABCB1* gene, are highly active in efflux-ion of drugs out of cells in a lipid-dependent manner [31].

The question then arose as to why the down-regulation of mitochondrial activity specifically induces *ABCB1* gene expression. A search of the literature pointed to at least five articles reporting *ABCB1* gene induction in response to mitochondrial activity down-regulation [32–36]. In conjunction with our results, this literature suggests that there is a direct inverse relationship between mitochondrial activity, *ABCB1* gene expression and tumour resistance to chemotherapy.

However, none of these published studies allude to the molecular mechanism linking altered mitochondrial activity to *ABCB1* gene activation.

To answer this question, one obvious avenue was that shutting down mitochondrial activity, means also a down-regulating lipid β-oxidation, which takes place in the mitochondrial matrix. The impairment of β-oxidation should therefore in turn promote lipid accumulation in cells due to the persistence of DNL and the import of dietary lipids. To test this hypothesis, we inhibited DNL with ACC1-specific inhibitor, ND-630, which is the first DNL enzyme. Remarkably, DNL inhibition completely abolished *ABCB1* activation in cells lacking mitochondria, indicating that some DNL products could be used to signal *ABCB1* activation to a transcription factor. To reinforce this hypothesis, we also tested octanoate, a medium-chain saturated fatty acid, which is also a dietary fat, freely entering cells and mitochondria and feeding the β-oxidation.

Interestingly, in our T-ALL cell models, octanoate treatment induced no cellular response in terms of *ABCB1* gene activation, but concomitant inhibition of β-oxidation and octanoate treatment effectively induced this gene, even in the presence of active, functional mitochondria. This observation suggests that octanoate itself can induce the *ABCB1* gene response, and that its degradation by β-oxidation competitively prevents its ability to mediate the *ABCB1* gene response by eliminating the available octanoate pool. A search of the literature for transcription factors capable of being activated by octanoate highlighted the lipogenic transcription factors, LXRα [27].

To test the hypothesis that LXRs are involved in *ABCB1* gene activation, we used the well-characterized LXR agonist GW3965, which effectively activated *ABCB1*, without the need for mitochondrial depletion. These data confirm that, in the absence of significant mitochondrial activity and hence lipid β-oxidation, accumulating lipids, particularly medium-chain saturated fatty acids, are able to activate LXR transcription factors, which in turn activate the *ABCB1* gene, leading to the establishment of effective acquired resistance to induction chemotherapy.

Our results also indicate that LXR transcription factors are activated by medium-chain saturated fatty acids, a previously overlooked property. It is well known that LXRs control the cellular cholesterol pool. LXR transcription factors are activated by physiological ligands such as oxysterols and cholesterol synthesis intermediates [28] and activate a series of ABC transporter genes such as *ABCA1*, which plays a determinant role in reverse cholesterol transport [37]. Interestingly, in agreement with our data, it has been shown that in early T-cell acute lymphoblastic leukemia (ETP-ALL), increased lipid synthesis and intracellular cholesterol pool, which are strong activators of LXRα transcription factor, are important pro-oncogenic events [38]. Although these investigations did not consider the LXRα-dependent oncogenic mechanisms, our data strongly suggest that the activation of *ABCB1* could be one of them.

We therefore propose that in the pathological context of T-ALL, in the absence of active lipid β-oxidation, the initial modest activation of LXR factors by the limited intermediate products of DNL, encompassing medium chain acyl-CoAs, could establish a vicious circle of lipogenic events since LXR activation could in turn activate genes encoding other lipogenic transcription factors such as SREBP1C and lipogenic enzymes such as FAS and ACC1 [28], leading to significant accumulation of fat in the form of lipid droplets in T-ALL cells with low mitochondrial activity.

Consequently, our work suggests that inhibiting DNL in MRD-positive patients, who predominantly harbor mitochondria-depleted T-ALL, could be a therapeutically attractive option. In addition, these patients should avoid diets and dietary supplements containing intermediate-chain saturated fatty acids such as caprylic acid (octanoate).

Conclusion

Our work demonstrated that in adult T-ALL, diminished mitochondrial function conferred chemoresistance to the cells by upregulating the expression of *ABCB1*, a key member of the ATP-binding cassette (ABC) transporter family. This regulation is mediated through enhanced lipid accumulation, reduced β-oxidation, and the subsequent activation of lipogenic transcription factors LXRs. These insights reveal a critical metabolic vulnerability in aggressive T-ALL. Based on these findings, we propose that therapeutic strategies targeting de novo lipogenesis and restricting dietary fats, such as caprylic acid, may mitigate treatment resistance and improve outcomes for patients with low mitochondrial activity in T-ALL.

Abbreviations

ABC	ATP-binding cassette
abn	Abnormalities
AcCoA	Acetyl-Coenzyme A
ACC1	Acetyl-CoA carboxylase 1
ANC	Absolute neutrophil count
Ara-C	Cytarabine
BM	Bone marrow
BSA	Bovine Serum Albumine
CAP	Chloramphenicol
GEC	Gene expression classifier
CI	Confidence interval
CK	Complex karyotype
CNS	Central nervous system
COX2	Cytochrome C Oxidase subunit 2
CR	Complete remission
DMSO	Dimethylsulfoxide
DNL	De novo lipid synthesis
EtBr	Ethidium bromide
ETC	Electron transport chain
ETP	Early T cell precursor
ETP-ALL	Early T-cell acute lymphoblastic leukemia
F	Female
FA	Fatty acids
FACS	Fluorescence-activated cell sorting
FBS	Fetal bovine serum
FDR	False Discovery Rate
GSEA	Gene Set Enrichment Analysis
HB	Hemoglobin
HSCT	Hematopoietic stem cell transplantation
IQR	Interquartile range
LEG-FABO+	Fatty-Acid-Beta-Oxidation positive
LEG-FABO-	Fatty-Acid-Beta-Oxidation negative
LXRs	Liver X receptors
M	Male
MDR1	Multidrug resistance factor 1
MRD	Minimal residual disease
MT+	High mitochondrial ETC activity
MT-	Low mitochondrial ETC activity
mtDNA	Mitochondrial DNA
NA	Not available
NUMTs	Nuclear mitochondrial DNA sequences
Oct	Octanonate
OS	Overall survival
PCA	Principal Component Analysis
PLT	Platelet
P-gp	P-glycoprotein
Rano	Ranolazine-2HCl
RT	Room temperature
TBST	Tris-buffered saline with 0.1% Tween 20 detergent
T-ALL	T-cell acute lymphoblastic leukemia
VCR	Vincristine sulfate
WBC	White blood cell

Supplementary Information

The online version contains supplementary material available at https://doi.org/10.1186/s12967-025-06423-4.

Additional file 1

Additional file 2

Additional file 3

Additional file 4

Additional file 5

Acknowledgements

We would like to thank every colleague in J. M.'s and S. K.'s labs for their invaluable contributions. We also thank the participants and their families for their willingness to contribute to this research, as well as the ethical review board for their guidance throughout the process. This work would not have been accomplished without the collaborative efforts of the entire team.

Author contributions

S. G. conducted the majority of the experiments, collected the clinical biological samples and performed statistical analyses. E. B.-F., F. C., and S. R. were responsible for performing and analysing all bioinformatics data, and helped with data interpretation. L.P. assisted in the collection of clinical information on patients with T-ALL. D.J. and J.M. contributed to discussions and provided research support. J.W. and S.K. co-designed this program and supervised this manuscript preparation. J.W. handled ethics committee procedures and registration of clinical trials, and supervised the clinical component of the program. All authors read and approved the final version of this manuscript.

Funding

This work was financially supported by National Natural Science Foundation of China (No. 82270187), Noncommunicable Chronic Diseases-National Science and Technology Major Project (No. 2023ZD0501300) and National Key R&D Program of China (No. 2023YFC2508900). S.K.'s laboratory was supported by the Cancer ITMO [Multi-Organisation Thematic Institute of the French Alliance for Life Sciences and Health (AVIESAN)] MIC program and Agence Nationale de la Recherche (ANR-23-CE12-0028-01 and ANR-23-CE14-0050-02).

Availability of data and materials
RNA-seq raw sequencing data (n = 79) generated in our study have been deposited in the GEO repository (GSE280250: https://www.ncbi.nlm.nih.gov/geo/query/acc.cgi?acc=GSE280250). RNA-seq data from 38 samples in our new 79-sample cohort were also analyzed in an independent study. The results of that study were recently published in *Wang* et al. [39] while this manuscript was under review. Additionally, previously published data from adult T-ALL patients enrolled in our center (n = 54) used for this study are available in *Chen* et al. [7], and *Peng* et al. [8]. Unprocessed blots are provided in Supplementary Source Data file 1. Other relevant materials used and analysed in this program are accessible through the corresponding author upon reasonable request.

Declarations

Ethics approval and consent to participate
All procedures performed in this study involving human samples were approved by the Ethics Review Committee of Ruijin Hospital, Shanghai Jiao Tong University School of Medicine, and in accordance with the Declaration of Helsinki. Each patient included in this study, or their families, provided informed consent by signing a consent form permitting the use of biomaterials and clinical data for scientific research purposes.

Consent for publication
Not applicable.

Competing interests
All the authors declare no competing interests.

Author details
[1]Shanghai Institute of Hematology, State Key Laboratory of Medical Genomics, National Research Center for Translational Medicine at Shanghai, Ruijin Hospital Affiliated to Shanghai Jiao Tong University School of Medicine, Shanghai 200025, China. [2]Univ. Grenoble Alpes, CNRS UMR 5309 and INSERM U1209, Institute for Advanced Biosciences, 38706 La Tronche, France. [3]Pôle Franco-Chinois de Recherche en Sciences du Vivant Et Génomique, Shanghai 200025, China.

Received: 17 January 2025 Accepted: 25 March 2025
Published online: 14 May 2025

References

1. Steimle T, Dourthe ME, Alcantara M, Touzart A, Simonin M, Mondesir J, et al. Clinico-biological features of T-cell acute lymphoblastic leukemia with fusion proteins. Blood Cancer J. 2022;12(1):14.
2. Girardi T, Vicente C, Cools J, De Keersmaecker K. The genetics and molecular biology of T-ALL. Blood. 2017;129(9):1113–23.
3. Genesca E, Gonzalez-Gil C. Latest contributions of genomics to T-cell acute lymphoblastic leukemia (T-ALL). Cancers (Basel). 2022;14(10):2474.
4. Gokbuget N, Boissel N, Chiaretti S, Dombret H, Doubek M, Fielding AK, et al. Diagnosis, prognostic factors and assessment of ALL in adults: 2023 ELN recommendations from a European expert panel. Blood. 2024;143:1891–902.
5. Pagliaro L, Chen SJ, Herranz D, Mecucci C, Harrison CJ, Mullighan CG, et al. Acute lymphoblastic leukaemia. Nat Rev Dis Primers. 2024;10(1):41.
6. Sentis I, Gonzalez S, Genesca E, Garcia-Hernandez V, Muinos F, Gonzalez C, et al. The evolution of relapse of adult T cell acute lymphoblastic leukemia. Genome Biol. 2020;21(1):284.
7. Chen B, Jiang L, Zhong ML, Li JF, Li BS, Peng LJ, et al. Identification of fusion genes and characterization of transcriptome features in T-cell acute lymphoblastic leukemia. Proc Natl Acad Sci USA. 2018;115(2):373–8.
8. Peng LJ, Zhou YB, Geng M, Bourova-Flin E, Chuffart F, Zhang WN, et al. Ectopic expression of a combination of 5 genes detects high risk forms of T-cell acute lymphoblastic leukemia. BMC Genomics. 2022;23(1):467.
9. Alaggio R, Amador C, Anagnostopoulos I, Attygalle AD, Araujo IBO, Berti E, et al. The 5th edition of the World health organization classification of haematolymphoid tumours: lymphoid neoplasms. Leukemia. 2022;36(7):1720–48.
10. Popow J, Alleaume AM, Curk T, Schwarzl T, Sauer S, Hentze MW. FASTKD2 is an RNA-binding protein required for mitochondrial RNA processing and translation. RNA. 2015;21(11):1873–84.
11. de Almeida MJ, Luchsinger LL, Corrigan DJ, Williams LJ, Snoeck HW. Dye-independent methods reveal elevated mitochondrial mass in hematopoietic stem cells. Cell Stem Cell. 2017;21(6):725–9 e4.
12. Ye J, Coulouris G, Zaretskaya I, Cutcutache I, Rozen S, Madden TL. Primer-BLAST: a tool to design target-specific primers for polymerase chain reaction. BMC Bioinformatics. 2012;13:134.
13. Dobin A, Davis CA, Schlesinger F, Drenkow J, Zaleski C, Jha S, et al. STAR: ultrafast universal RNA-seq aligner. Bioinformatics. 2013;29(1):15–21.
14. Anders S, Pyl PT, Huber W. HTSeq–a Python framework to work with high-throughput sequencing data. Bioinformatics. 2015;31(2):166–9.
15. Behdenna A, Colange M, Haziza J, Gema A, Appe G, Azencott CA, et al. pyComBat, a Python tool for batch effects correction in high-throughput molecular data using empirical Bayes methods. BMC Bioinformatics. 2023;24(1):459.
16. Rath S, Sharma R, Gupta R, Ast T, Chan C, Durham TJ, et al. MitoCarta3.0: an updated mitochondrial proteome now with sub-organelle localization and pathway annotations. Nucleic Acids Res. 2021;49(D1):D1541–7.
17. Subramanian A, Tamayo P, Mootha VK, Mukherjee S, Ebert BL, Gillette MA, et al. Gene set enrichment analysis: a knowledge-based approach for interpreting genome-wide expression profiles. Proc Natl Acad Sci USA. 2005;102(43):15545–50.
18. Mootha VK, Lindgren CM, Eriksson KF, Subramanian A, Sihag S, Lehar J, et al. PGC-1alpha-responsive genes involved in oxidative phosphorylation are coordinately downregulated in human diabetes. Nat Genet. 2003;34(3):267–73.
19. Liberzon A, Birger C, Thorvaldsdottir H, Ghandi M, Mesirov JP, Tamayo P. The molecular signatures database (MSigDB) hallmark gene set collection. Cell Syst. 2015;1(6):417–25.
20. Fang Z, Liu X, Peltz G. GSEApy: a comprehensive package for performing gene set enrichment analysis in Python. Bioinformatics. 2023;39(1):btac757.
21. Neupert W. Mitochondrial gene expression: a playground of evolutionary tinkering. Annu Rev Biochem. 2016;85:65–76.
22. Herranz D, Ambesi-Impiombato A, Sudderth J, Sanchez-Martin M, Belver L, Tosello V, et al. Metabolic reprogramming induces resistance to anti-NOTCH1 therapies in T cell acute lymphoblastic leukemia. Nat Med. 2015;21(10):1182–9.
23. Callaghan R, Crowley E, Potter S, Kerr ID. P-glycoprotein: so many ways to turn it on. J Clin Pharmacol. 2008;48(3):365–78.
24. Kramer NJ, Prakash G, Isaac RS, Choquet K, Soto I, Petrova B, et al. Regulators of mitonuclear balance link mitochondrial metabolism to mtDNA expression. Nat Cell Biol. 2023;25(11):1575–89.
25. Mathiowetz AJ, Olzmann JA. Lipid droplets and cellular lipid flux. Nat Cell Biol. 2024;26(3):331–45.
26. McDonnell E, Crown SB, Fox DB, Kitir B, Ilkayeva OR, Olsen CA, et al. Lipids reprogram metabolism to become a major carbon source for histone acetylation. Cell Rep. 2016;17(6):1463–72.
27. Bedi S, Hines GV, Lozada-Fernandez VV, de Jesus PC, Kaliappan A, Rider SD Jr, et al. Fatty acid binding profile of the liver X receptor alpha. J Lipid Res. 2017;58(2):393–402.
28. Wang Y, Viscarra J, Kim SJ, Sul HS. Transcriptional regulation of hepatic lipogenesis. Nat Rev Mol Cell Biol. 2015;16(11):678–89.
29. Wagner BL, Valledor AF, Shao G, Daige CL, Bischoff ED, Petrowski M, et al. Promoter-specific roles for liver X receptor/corepressor complexes in the regulation of ABCA1 and SREBP1 gene expression. Mol Cell Biol. 2003;23(16):5780–9.
30. Morrish E, Copeland A, Moujalled DM, Powell JA, Silke N, Lin A, et al. Clinical MDR1 inhibitors enhance Smac-mimetic bioavailability to kill murine LSCs and improve survival in AML models. Blood Adv. 2020;4(20):5062–77.
31. Hegedus C, Telbisz A, Hegedus T, Sarkadi B, Ozvegy-Laczka C. Lipid regulation of the ABCB1 and ABCG2 multidrug transporters. Adv Cancer Res. 2015;125:97–137.
32. Lee W, Choi HI, Kim MJ, Park SY. Depletion of mitochondrial DNA upregulates the expression of MDR1 gene via an increase in mRNA stability. Exp Mol Med. 2008;40(1):109–17.

33. Yu M, Shi Y, Wei X, Yang Y, Zang F, Niu R. Mitochondrial DNA depletion promotes impaired oxidative status and adaptive resistance to apoptosis in T47D breast cancer cells. Eur J Cancer Prev. 2009;18(6):445–57.
34. Perez MJ, Gonzalez-Sanchez E, Gonzalez-Loyola A, Gonzalez-Buitrago JM, Marin JJ. Mitochondrial genome depletion dysregulates bile acid- and paracetamol-induced expression of the transporters Mdr1, Mrp1 and Mrp4 in liver cells. Br J Pharmacol. 2011;162(8):1686–99.
35. Gonzalez-Sanchez E, Marin JJ, Perez MJ. The expression of genes involved in hepatocellular carcinoma chemoresistance is affected by mitochondrial genome depletion. Mol Pharm. 2014;11(6):1856–68.
36. Rowe SP, Gorin MA, Solnes LB, Ball MW, Choudhary A, Pierorazio PM, et al. Correlation of (99m)Tc-sestamibi uptake in renal masses with mitochondrial content and multi-drug resistance pump expression. EJNMMI Res. 2017;7(1):80.
37. Moore JM, Bell EL, Hughes RO, Garfield AS. ABC transporters: human disease and pharmacotherapeutic potential. Trends Mol Med. 2023;29(2):152–72.
38. Rashkovan M, Albero R, Gianni F, Perez-Duran P, Miller HI, Mackey AL, et al. Intracellular cholesterol pools regulate oncogenic signaling and epigenetic circuitries in early T-cell precursor acute lymphoblastic leukemia. Cancer Discov. 2022;12(3):856–71.
39. Wang JY, Gui TT, Jiao B, Liu X, Ma XL, Wang C, et al. Metabolomic insights into pathogenesis and therapeutic potential in adult acute lymphoblastic leukemia. Proc Natl Acad Sci USA. 2025;122(7): e2423169122.

Publisher's Note